ELSEVIER

Thermochimica Acta 400 (2003) 235–245

thermochimica acta

www.elsevier.com/locate/tca

Thermochemical decomposition of cobalt doped ammonium paratungstate precursor

Zongyin Zhang*, Mamoun Muhammed

Department of Materials Science and Engineering, Royal Institute of Technology, SE-100 44 Stockholm, Sweden

Received 15 January 2002; received in revised form 4 October 2002; accepted 14 October 2002

Abstract

The calcination is one of the important steps in the preparation of nanostructured WC and WC–Co powders from chemically co-precipitated W–Co precursors. In the present paper, the processing of the precursor prepared by co-precipitation from cobalt(II) hydroxide and ammonium paratungstate is reported. The precursor was calcined at different temperatures under various atmospheres. The resulting powders were investigated using scanning electron microscopy, X-ray diffraction, thermogravimetric analysis (TGA), differential TGA, BET, and mass spectrographic analysis techniques. The results showed that the precursor decomposes differently by calcination under different atmospheres, i.e. nitrogen, air, and helium–5% oxygen. Different decomposition behaviour was observed when the calcination was carried out at medium temperature in flowing and non-flowing air. Nanostructured powders with particle size of around 90 nm can be obtained after calcination. The precursor decomposes into $CoWO_4$ and WO_3 oxides at 520 °C in air after a weight loss of 10.3%.

Keywords: W–Co precursor; Chemical synthesis; Decomposition; Calcination temperature; Calcination atmosphere

1. Introduction

WC–Co hard materials are widely used in the production of cutting-, drilling-, and forming-tool materials because they have a high hardness and wear resistance, good resistance to high temperatures, and good toughness. In the conventional method of producing WC–Co materials, tungsten carbide powder obtained from the reduction of tungsten is mixed with cobalt by milling, and then followed by crushing, pressing, and sintering to form sintered products. Currently ammonium paratungstate (APT) is the dominating raw material used for the manufacture of tungsten-based products. Tungsten powders are prepared by hydrogen reduction of APT as well as tungsten blue oxide (TBO) or other tungsten oxides obtained from APT [1–5].

The calcination of APT is one of the important processes in the preparation of tungsten powder. The use of different calcination conditions leads to the formation of different products [6–10], which affects the reduction and carburization processes. During the calcination of APT, tungsten trioxide (WO_3) is formed at temperature above 400 °C under oxidizing conditions (i.e. air) [8,9]. TBO is formed at a similar temperature [2,11] under slightly reducing conditions, i.e. hydrogen or a hydrogen–nitrogen gas mixture. TBO consists of several different phases such as ammonium and hydrogen bronze (ATB, HTB), WO_3, tungsten β-oxide ($WO_{2.9}$), tungsten γ-oxide ($WO_{2.72}$), tungsten dioxide

* Corresponding author. Tel.: +46-8-7906544; fax: +48-8-207681.
E-mail address: zongyinz@met.kth.se (Z. Zhang).

0040-6031/03/$ – see front matter
PII: S0040-6031(02)00499-9

(WO_2) and β-tungsten (W_3O). Reducing conditions can also be obtained with the use of inert gas (e.g. nitrogen), since ammonia evolved from the powder partially cracks into nitrogen and hydrogen gas. Parameters such as temperature, heating time, composition and pressure of the atmosphere, gas flow, mass of APT flow with time, layer height in the boat (in the push-type furnace), and slope and rotation rate (rotary furnace) are very important parameters, which affect the calcination of the precursor [11]. Chemical composition, the ratio of crystalline to amorphous material, and the internal porosity of the particles are dependent on the calcination conditions. Schubert and Lassner [7] reported that the initial decomposition step is decisive in regulating the consistency and purity of the final tungsten powder quality. In this study, a maximum value of specific surface area was obtained at 400 °C, due to changes in the microporosity and in the surface structure.

Reducing the particle size in WC–Co hard materials improves mechanical properties such as increased hardness, transverse rupture strength, and compression strength [12]. Hence, the investigation of nanostructured WC–Co materials becomes a more interesting field. Several groups have studied the fabrication of nanostructured WC–Co materials [13–15], in order to obtain nanostructured hard materials with the improved properties, e.g. higher mechanical properties and better sinterability of sintered tungsten carbides.

The fabrication of nanostructured WC–Co powder includes precursor preparation and thermochemical conversion processes such as reduction and carburization [16,17]. The W–Co precursors are generally prepared by chemical synthesis methods, such as spray drying [18,19] and co-precipitation [20–23]. A co-precipitation method for the synthesis of cobalt doped ammonium paratungstate (Co-doped APT) precursors has been developed and patented [21,22]. Co-doped APT precursors have been found to be an analogy to APT with a nominal composition of $(NH_4)_{10-2x}Co_x(NH_3)_xH_2W_{12}O_{42}{\cdot}yH_2O$, in which paratungstate anions are surrounded by cobalt and ammonium ions as well as water and possibly ammonia molecules. Nanostructured WC–Co and W–Co powders have been produced using this precursor [16,24]. The thermal decomposition of crystalline APT and amorphous ammonium metatungstate (AMT) has been investigated [6,9]. The decomposition of APT showed that there are two transformations between amorphous and crystalline phases from room temperature to 450 °C, i.e. precursor (crystalline) → amorphous powder → oxides (crystalline). No study of the decomposition of Co-doped APT has been reported, though it is known that the Co-doped precursor has different properties from those of APT. As the calcination of APT is an important step in the production of tungsten powders, information on calcination products will be of importance in selecting a suitable processing route to convert the precursor into a nanostructured WC–Co powder. Therefore, the aim of the present study is to investigate the effect of calcination parameters, such as temperature and atmosphere, on the characteristics of the decomposition of Co-doped APT precursor made by co-precipitation. The decomposition reactions and phase constituents have been studied. Also, the properties of the calcined powders including particle size, microstructure, and specific surface area have particularly been studied.

2. Experimental

2.1. Materials and precursor synthesis

APT (>99% pure, Fluka, Switzerland) and cobalt(II) hydroxide ($Co(OH)_2$, >95% pure, Sigma-Aldrich, Sweden AB) were used as raw materials. The precursor with W/Co ratio of 4.7 was synthesized. Both salts are slightly soluble and were suspended in a stirred reactor containing water. The reaction mixture was heated to 90 °C for 3 h. After the reaction was completed, the solid powder formed was filtered off, washed with de-ioned water and dried in air at 105 °C. Composition and phase constituent were carried out on the formed powder by chemical analysis and X-ray diffraction (XRD), and it has been found that powder with W/Co ratio of 4.7 has a general composition of $(NH_4)_5Co_{2.5}(NH_3)_{2.5}H_2W_{12}O_{42}{\cdot}9H_2O$. More details of the precursor synthesis have been given elsewhere [21,22].

2.2. Calcination of the precursor

The precursor was calcined at several constant temperatures between 220 and 650 °C for 5 h with varying gas phase conditions, i.e. flowing air, flowing nitrogen,

and non-flowing air. The calcination was carried out in a tube furnace. The heating rate of the samples from room temperature to the calcination temperature was 5 °C/min. A gas flow rate of 800 ml/min was used during calcination. Air and nitrogen used in the study had purities of >99.99% (Air Liquid Company, Sweden).

2.3. Characterization of the powders

The thermal decomposition of the precursor was studied by measuring the weight loss as a function of temperature in air using a TGA 7 thermogravimetric analyser (Perkin-Elmer), and differential TGA (DTGA) pattern was also obtained. The heating rate was 5 °C/min in the temperature range between 50 and 800 °C. The morphology of calcined powders was examined using scanning electron microscopy (SEM) (Jeol JSM-840). The phases formed in the powder were identified by XRD using a Philips PW 1012/20 X-ray Diffractometer with Cu Kα1 radiation. The diffraction database, International Centre for Diffraction Data, Join Committee on Powder Diffraction Standards (JCPDS), Swarthmore, USA, 1997, was used for phase identification. The specific surface area of the powders was measured by nitrogen absorption according to the BET method using a Micrometric Gemini 2360 instrument. The density of some calcined powders was measured using a Gemini AccuPyc 1330 pycnometer. The particle size of some calcined powder was calculated from data of specific surface area and measured density. Residual gas analysis, water and ammonia, from the decomposition of the precursor were evaluated using a temperature programmed decomposition reactor (TPR) with a mass spectrometer (MimiLab LM80) as a detector. The heating rate was 5 °C/min in the temperature range between 50 and 650 °C. The decomposition was carried out under different atmospheres, i.e. air, nitrogen, and helium–5% oxygen, which were >99.99% pure products of Air Liquid Company, Sweden.

3. Results and discussion

3.1. Decomposition

The thermal decomposition of the precursor with an initial composition of $(NH_4)_5Co_{2.5}(NH_3)_{2.5}H_2W_{12}O_{42}\cdot 9H_2O$ was studied by measuring the weight loss in air as a function of temperature. TGA and DTGA curves are presented in Fig. 1. The decomposition of the precursor under different gas phase conditions was also studied, and the TPR curve is shown in Fig. 2. The decomposition of the precursor under different gas phase conditions produces different compositions. The different relative areas of each peak in the TPR

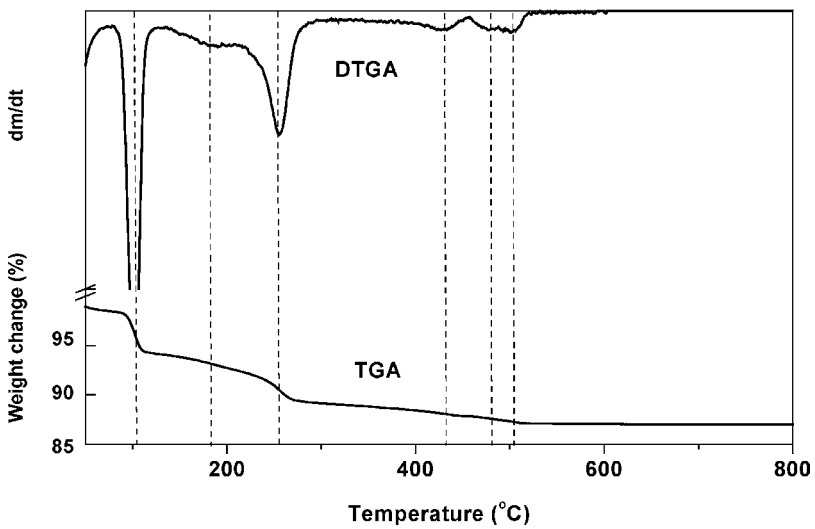

Fig. 1. TGA and DTGA curves of the precursor.

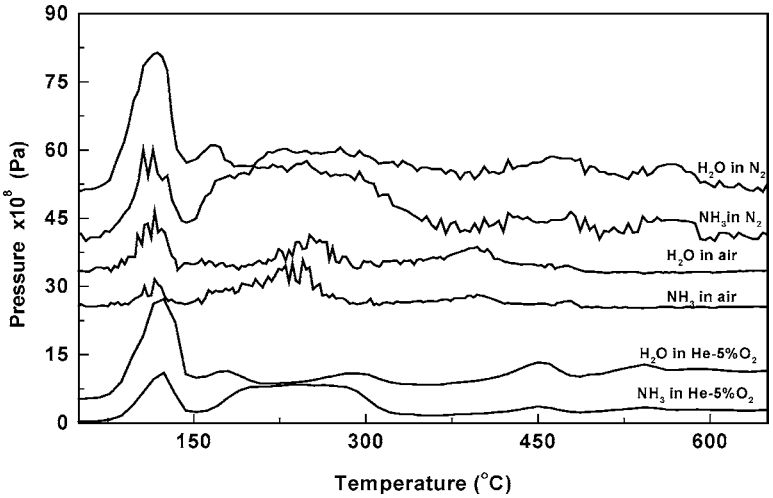

Fig. 2. Analysis of H_2O and NH_3 produced as a result of the decomposition of the precursor in three different gas phases.

curves indicate that different amounts of water and ammonia are produced. This is a result of different decomposition reactions taking place in different atmospheres. In general, the decomposition of the precursor under gas phases can be divided into five main parts. The temperature range of every step and the decomposition (reaction) are different under three gas phase conditions.

From TGA, DTGA and TPR results, the decomposition of the precursor in air can be identified as five steps. At temperatures below 100 °C, the water absorbed on the surface of the precursor is released, and the weight loss is 2.7%. In five steps, different amounts of water and ammonia were released, and different weight losses were obtained. The total weight loss during the whole decomposition process is 10.3%. The temperature range of every step during the decomposition of the precursor in air, helium–5% oxygen, nitrogen is given in Table 1. Weight loss of the precursor during decomposition in different temperature ranges under air is also given in Table 1. The gas phase composition in contact with the samples does not seem to affect the decomposition in the initial two steps.

In the first step (90–125 °C), the decomposition reaction can be written as:

$$(NH_4)_5Co_{2.5}(NH_3)_{2.5}H_2W_{12}O_{42} \cdot 9H_2O \rightarrow (NH_4)_5Co_{2.5}H_2W_{12}O_{42} \cdot 5H_2O + 2.5NH_3 + 4H_2O \quad (1)$$

The second decomposition step takes place between 125 and 210 °C, and amorphous powder starts to form in this step:

$$(NH_4)_5Co_{2.5}H_2W_{12}O_{42} \cdot 5H_2O \rightarrow (NH_4)_4Co_{2.5}H_2W_{12}O_{41.5} \cdot 3.5H_2O \text{ (amorphous)} + 2H_2O + NH_3 \quad (2)$$

Table 1
Summary of the observed temperature ranges (°C) for different decomposition steps of the precursor under different atmospheres and weight loss in air

	Step 1	Step 2	Step 3	Step 4	Step 5
Air	90–125	125–210	210–300	300–450	450–520
Helium–5% oxygen	90–125	125–210	210–350	350–480	480–570
Nitrogen	90–125	125–210	210–400	400–500	500–610
Weight loss in air (%)	3.3	1.5	3.4	1.7	0.4

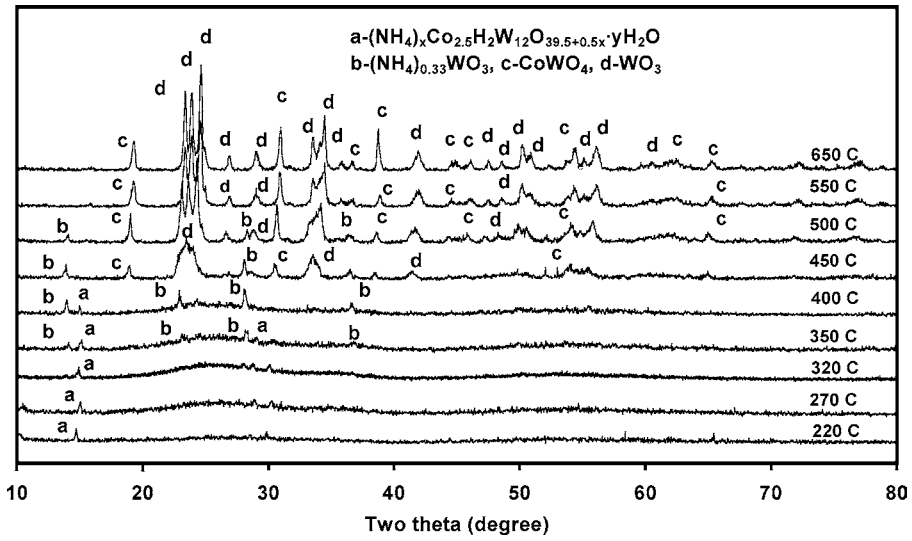

Fig. 3. XRD spectra of the powders calcined at different temperatures under flowing air.

In the third step the product was mainly amorphous powder. The appearance of an amorphous phase has been identified by XRD. Figs. 3–5 show the XRD spectra of the powders calcined at different temperatures under flowing air, flowing nitrogen, and non-flowing air, respectively. However, very small amount of crystalline phase exists up to 400 °C, whose composition can be expressed as $(NH_4)_xCo_{2.5}H_2W_{12}O_{39.5+0.5x} \cdot yH_2O$, which varies with temperature. The decomposition in air (210–300 °C) is given

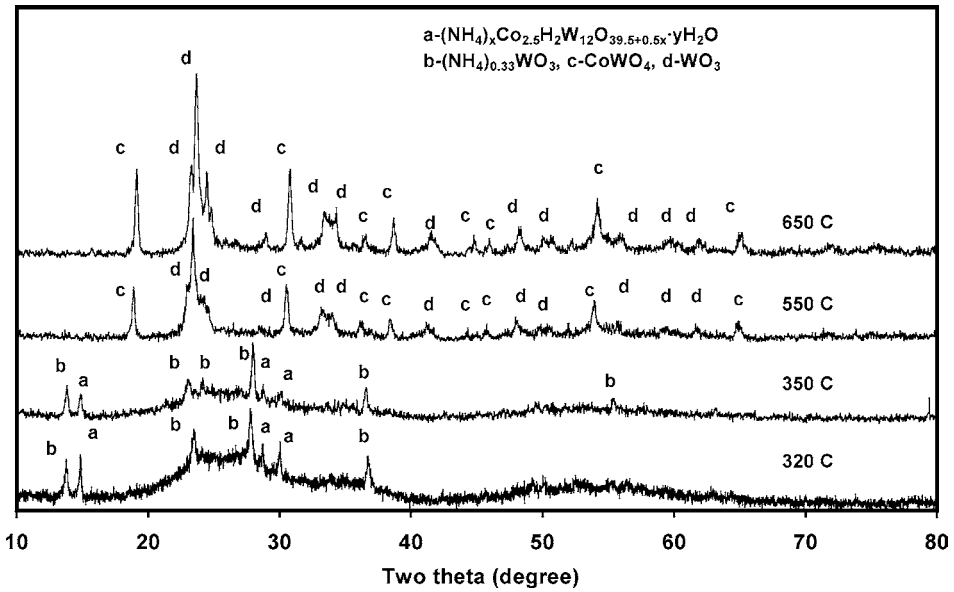

Fig. 4. XRD spectra of the powders calcined at different temperatures under flowing nitrogen.

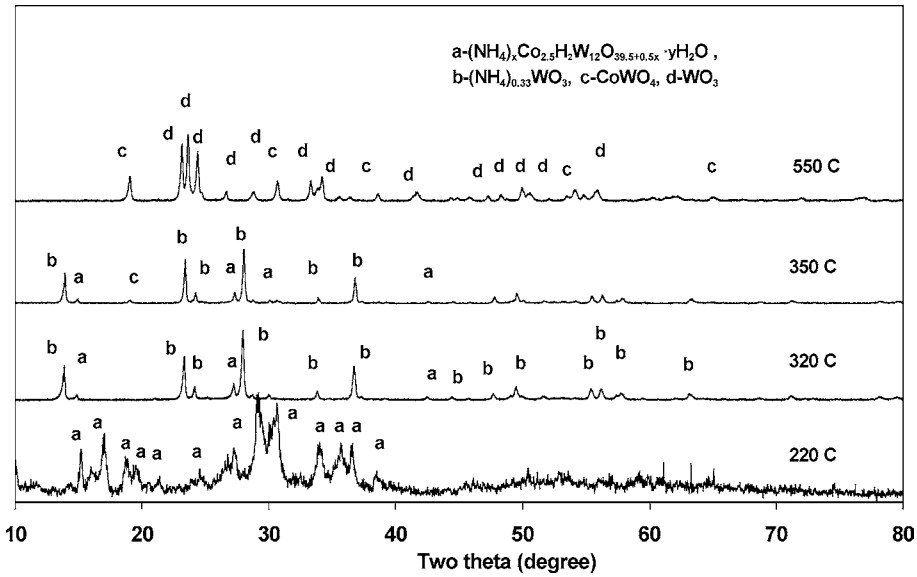

Fig. 5. XRD spectra of calcined powders under non-flowing air.

in Eq. (3):

$$(NH_4)_4Co_{2.5}H_2W_{12}O_{41.5} \cdot 3.5H_2O \text{ (amorphous)} \rightarrow (NH_4)_2Co_{2.5}H_2W_{12}O_{40.5} \text{ (amorphous)} + 2NH_3 + 4.5H_2O \quad (3)$$

Another reaction occurs at temperatures above 300 °C, which does not cause any weight loss:

$$(NH_4)_2Co_{2.5}H_2W_{12}O_{40.5} \text{ (amorphous)} \rightarrow x(NH_4)_{0.33}WO_3 + (NH_4)_{2-0.33x}Co_{2.5}H_2W_{12-x}O_{40.5-3x} \text{ (amorphous)} \quad (4)$$

At higher temperatures, the decomposition reaction and the temperatures seem to be dependent on the gas phase used. The decomposition of the precursor in nitrogen (210–400 °C) or helium–5% oxygen (210–350 °C) produces another amorphous powder. This reaction can be expressed in Eq. (5):

$$(NH_4)_4Co_{2.5}H_2W_{12}O_{41.5} \cdot 3.5H_2O \text{ (amorphous)} \rightarrow (NH_4)_{2-0.33x}Co_{2.5}H_2W_{12-x}O_{40.5-3x} \text{ (amorphous)} + x(NH_4)_{0.33}WO_3 + 2NH_3 + 4.5H_2O \quad (5)$$

Reaction (4) seems to occur in different temperature ranges depending on the gas phase composition. $(NH_4)_{0.33}WO_3$ was reported by Fouad et al. [25] during decomposition of APT under hydrogen, which can exist at temperatures between 250 and 575 °C. In the present study, the $(NH_4)_{0.33}WO_3$ phase appears in the sample calcined at 350 °C under flowing air and exists until 500 °C. $(NH_4)_{0.33}WO_3$ appears at 320 °C when the samples were calcined under flowing nitrogen and non-flowing air, as shown in Figs. 3–5. Almost only $(NH_4)_{0.33}WO_3$ was detected in the sample calcined at 320 °C under non-flowing air. $(NH_4)_{0.33}WO_3$ was formed at higher temperatures when the samples were calcined under flowing air than under flowing nitrogen. The amount of $(NH_4)_{0.33}WO_3$ also varies with calcination temperature, time, and atmosphere. The formation of $(NH_4)_{0.33}WO_3$ could not be observed by TGA (Fig. 1) because reaction (4) occurs without any weight change.

During the fourth step the further decomposition of the samples proceeds differently, depending on the composition of the gas phase. The following reaction takes place in air (300–450 °C):

$$(NH_4)_2Co_{2.5}H_2W_{12}O_{40.5} \text{ (amorphous)} \rightarrow (NH_4)_{0.5-0.33x}Co_{2.5}W_{12-x}O_{38.75-3x} \text{ (amorphous)} + x(NH_4)_{0.33}WO_3 + 1.5NH_3 + 1.75H_2O \quad (6)$$

While the decomposition under helium–5% oxygen (350–480 °C):

$$(NH_4)_{2-0.33x}Co_{2.5}H_2W_{12-x}O_{40.5-3x}\ \text{(amorphous)} \rightarrow (NH_4)_{0.5-0.33x}Co_{2.5}W_{12-x}O_{38.75-3x}\ \text{(amorphous)} + 1.5NH_3 + 1.75H_2O \quad (7)$$

The decomposition of the precursor under nitrogen (400–500 °C) yields:

$$(NH_4)_{2-0.33x}Co_{2.5}H_2W_{12-x}O_{40.5-3x} \rightarrow (NH_4)_{1-0.33x}Co_{2.5}W_{12-x}O_{39-3x}\ \text{(amorphous)} + NH_3 + 1.5H_2O \quad (8)$$

The observed weight loss of the sample in the final decomposition step can be attributed to a further loss of water and ammonia. The final products, $CoWO_4$ and WO_3 were obtained. In air (450–520 °C) and helium–5% oxygen (480–570 °C):

$$(NH_4)_{0.5-0.33x}Co_{2.5}W_{12-x}O_{38.75-3x}\ \text{(amorphous)} + x(NH_4)_{0.33}WO_3 \rightarrow 2.5CoWO_4 + 9.5WO_3 + 0.5NH_3 + 0.25H_2O \quad (9)$$

From the TGA and DGTA curves, it seems to be two sub-reactions occurring in this step. One occurs between 450 and 500 °C, and another is between 500 and 520 °C. The study indicated that the decomposition of $(NH_4)_{0.33}WO_3$ into WO_3 under air at 500 °C [26]. Hence, it is possible that WO_3 is formed from the decomposition of $(NH_4)_{0.33}WO_3$ at 500 °C.

The decomposition of the precursor under nitrogen (500–610 °C) is given by:

$$(NH_4)_{1-0.33x}Co_{2.5}W_{12-x}O_{39-3x} + x(NH_4)_{0.33}WO_3 \rightarrow 2.5CoWO_4 + 9.5WO_3 + NH_3 + 0.5H_2O \quad (10)$$

The decomposition temperature of the precursor in each step under flowing air is lower than that under flowing nitrogen, which is agreeable with the results of APT decomposition [27]. The studies of the decomposition of APT under hydrogen and nitrogen [6,8,9] showed that the decomposition results in the formation of WO_3 at temperatures between 400 and 500 °C. In the present case, WO_3 and $CoWO_4$ were formed during calcination under flowing air at 450 °C. The final temperature at which the precursor completely decomposes to WO_3 and $CoWO_4$ is 520 °C, a slightly higher than that of APT. However, complete decomposition of the precursor under a flowing nitrogen atmosphere requires temperature as high as 610 °C. The reason, perhaps, is that $CoWO_4$ formation and $(NH_4)_{0.33}WO_3$ decomposition into WO_3 need higher temperatures.

3.2. Identification of phase formed

Table 2 summarizes the phases identified in the different samples of the calcined powders. The composition of the compounds formed is deduced from TGA, TPR, and XRD experimental data. The structural change was followed as a function of temperature under flowing air, flowing nitrogen, and non-flowing air. The powders calcined at lower temperatures were mainly XRD amorphous under all atmospheres. Those calcined at higher temperatures were crystalline (when using flowing and non-flowing gases). The powders calcined under flowing nitrogen contained more crystalline phases than those calcined under flowing air at the same temperature. It can be seen from XRD spectra (Figs. 3 and 4), that the powders obtained under flowing air were mainly amorphous with a small fraction of $(NH_4)_xCo_{2.5}H_2W_{12}O_{39.5+0.5x} \cdot yH_2O$ up to 400 °C. At 350 °C, $(NH_4)_{0.33}WO_3$ appeared, and the powder was still amorphous with small amounts of $(NH_4)_xCo_{2.5}H_2W_{12}O_{39.5+0.5x} \cdot yH_2O$ and $(NH_4)_{0.33}WO_3$. $(NH_4)_xCo_{2.5}H_2W_{12}O_{39.5+0.5x} \cdot yH_2O$ phase disappeared at 450 °C. The peaks of $CoWO_4$ and WO_3 were observed in XRD spectra of the powders calcined at 450 °C, which is agreeable with TGA result. $(NH_4)_{0.33}WO_3$ disappeared at 550 °C, and only $CoWO_4$ and WO_3 were formed as final product.

The powders with the same phase constituents were produced during the decomposition of the precursor calcined at temperatures above 350 °C under flowing nitrogen and flowing air. $(NH_4)_{0.33}WO_3$ appeared at 320 °C under flowing nitrogen compared with 350 °C under flowing air. However, there existed a larger fraction of $(NH_4)_xCo_{2.5}H_2W_{12}O_{39.5+0.5x} \cdot yH_2O$ and $(NH_4)_{0.33}WO_3$ in the calcined powders at 320 and 350 °C under flowing nitrogen. Different phases were obtained under non-flowing air. The powder calcined at 220 °C contained very large amounts of the $(NH_4)_xCo_{2.5}H_2W_{12}O_{39.5+0.5x} \cdot yH_2O$ phase. Amorphous phase disappeared at 320 °C. The

Table 2
The composition of compound formed and colours of the powders after calcination at different temperatures

Parameters	Suggested composition of phase formed	Colour
Precursor	$(NH_4)_5Co_{2.5}(NH_3)_{2.5}H_2W_{12}O_{42} \cdot 9H_2O$	Pink
220 °C non-flowing air	Amorphous, $(NH_4)_xCo_{2.5}H_2W_{12}O_{39.5+0.5x} \cdot yH_2O$	Purplish pink
320 °C non-flowing air	$(NH_4)_xCo_{2.5}H_2W_{12}O_{39.5+0.5x} \cdot yH_2O$, $(NH_4)_{0.33}WO_3$	Yellow
350 °C non-flowing air	$(NH_4)_xCo_{2.5}H_2W_{12}O_{39.5+0.5x} \cdot yH_2O$, $(NH_4)_{0.33}WO_3$, $CoWO_4$	Yellow
550 °C non-flowing air	$CoWO_4$, WO_3	Light blue
320 °C flowing N_2	Amorphous, $(NH_4)_xCo_{2.5}H_2W_{12}O_{39.5+0.5x} \cdot yH_2O$, $(NH_4)_{0.33}WO_3$	Greenish blue
350 °C flowing N_2	Amorphous, $(NH_4)_xCo_{2.5}H_2W_{12}O_{42} \cdot yH_2O$, $(NH_4)_{0.33}WO_3$	Greenish blue
550 °C flowing N_2	$CoWO_4$, WO_3	Dark blue
650 °C flowing N_2	$CoWO_4$, WO_3	Dark blue
220 °C flowing air	Amorphous, $(NH_4)_xCo_{2.5}H_2W_{12}O_{39.5+0.5x} \cdot yH_2O$	Greenish blue
270 °C flowing air	Amorphous, $(NH_4)_xCo_{2.5}H_2W_{12}O_{39.5+0.5x} \cdot yH_2O$	Greenish blue
320 °C flowing air	Amorphous, $(NH_4)_xCo_{2.5}H_2W_{12}O_{39.5+0.5x} \cdot yH_2O$	Greenish blue
350 °C flowing air	Amorphous, $(NH_4)_xCo_{2.5}H_2W_{12}O_{39.5+0.5x} \cdot yH_2O$, $(NH_4)_{0.33}WO_3$	Greenish blue
400 °C flowing air	Amorphous, $(NH_4)_xCo_{2.5}H_2W_{12}O_{39.5+0.5x} \cdot yH_2O$, $(NH_4)_{0.33}WO_3$	Greenish blue
450 °C flowing air	Amorphous, $CoWO_4$, WO_3, $(NH_4)_{0.33}WO_3$	Greenish blue
500 °C flowing air	$CoWO_4$, WO_3, $(NH_4)_{0.33}WO_3$	Light blue
550 °C flowing air	$CoWO_4$, WO_3	Light blue
650 °C flowing air	$CoWO_4$, WO_3	Light blue

powders calcined at 320 and 350 °C mainly contained $(NH_4)_{0.33}WO_3$ phase with a small amount of $(NH_4)_xCo_{2.5}H_2W_{12}O_{39.5+0.5x} \cdot yH_2O$. $CoWO_4$ and WO_3 were formed at 550 °C.

The thermal decomposition of APT and AMT has been investigated [6,9]. The decomposition of APT showed that there are two-phase transformations between amorphous and crystalline states from room temperature to 450 °C, i.e. precursor (crystalline) → amorphous powder → oxides (crystalline). The precursor used in the present study has different properties from APT due to the presence of cobalt. Under the conditions of flowing air and flowing nitrogen used in the present experiment, the gas phase composition in the furnace is kept almost at a steady state during calcination. The vapour of water and ammonia from the precursor are removed by the flowing gases as soon as they are formed. Under non-flowing air, water and ammonia produced by the decomposition of the precursor affect the equilibrium between gas and solid in the furnace. The ammonia content in the furnace increases during the calcination under non-flowing air is higher than that under flowing air and flowing nitrogen.

The colour of the calcined powders was found to vary under the different conditions. Under flowing air and nitrogen, the colour of the powders changed from pink (precursor) to greenish blue (calcined at low and medium temperatures), light blue (in air), or dark blue (in nitrogen) (calcined at high temperatures) with increasing temperature. Under non-flowing air, the colour changed from pink (precursor) to purplish pink (at low temperatures), yellow (calcined at medium temperatures), or light blue (at high temperatures). The usual colours of tungsten oxides are yellow (WO_3), blue ($WO_{2.9}$), violet ($WO_{2.72}$), and brown (WO_2) [28]. The colour of $CoWO_4$ is blue-green [29]. It was reported that $WO_{2.9}$, $WO_{2.72}$, and WO_2 formation could affect the colour of the produced powder in the decomposition of APT and hydrogen reduction of the tungsten oxides [7]. In the present experiment, $WO_{2.9}$, $WO_{2.72}$, and WO_2 were not observed from XRD spectra. After the calcination at 220 °C under non-flowing air, the powder becomes purplish pink. The colour of the powders calcined at 320 and 350 °C resulted from the $(NH_4)_{0.33}WO_3$ phase. The light blue colour at 550 °C is from the $CoWO_4$. More $(NH_4)_{0.33}WO_3$ could be formed at 350 °C under non-flowing air than under flowing air. This leads to different colours: yellow under non-flowing air and greenish blue under flowing air. Light blue and dark blue colours were observed in the samples calcined at 650 °C under flowing air and flowing nitrogen respectively. A possible explanation

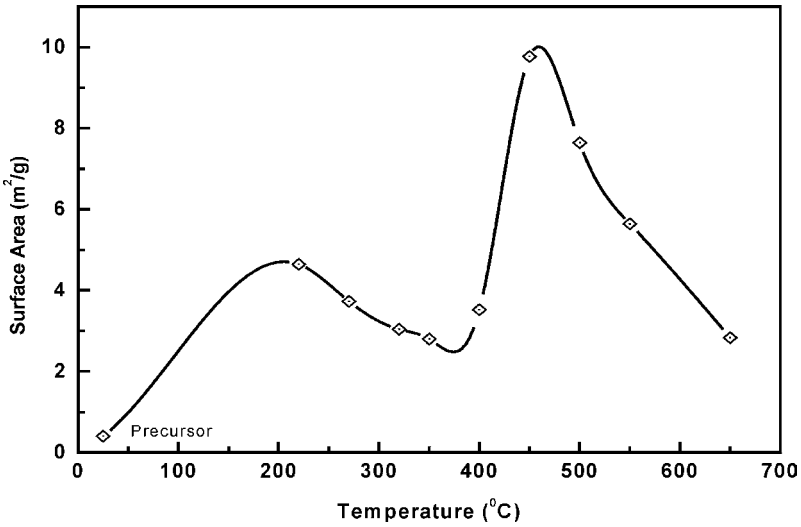

Fig. 6. Specific surface area of calcined powder under flowing air.

is that the powder calcined under flowing nitrogen contains more WO_{3-x} than those calcined under flowing air, though not enough to be detected by XRD.

3.3. The specific surface area and particle size of the powders

Fig. 6 and Table 3 show the specific surface area for different powder samples calcined under different conditions, which was measured by nitrogen adsorption according to the BET method. The specific surface area of the calcined powders was found to be a function of decomposition temperature and atmosphere. The changes in the specific surface area are related to a change in the composition and the crystal structure of the materials that were obtained at different calcined temperatures. An increase in the specific surface area can be observed as the materials are decomposed under the evolution of gases or when a new phase crystallizes.

Two maximum surface area values of 4.6 m^2/g at 220 °C and 9.8 m^2/g at 450 °C were observed for the powders calcined under flowing air. The powders calcined at medium temperatures under non-flowing air have much higher specific surface area values than those calcined under flowing air and nitrogen. The particle sizes of the powders calcined at 450 °C under flowing air and at 320 °C under non-flowing air were calculated from data of the specific surface area and density by presuming spherical particles. To calculate particle size of the powder calcined at 320 °C under non-flowing air and at 450 °C under flowing air, the density of two powders were measured, which were 7.36 and 7.58 g/cm^3, respectively. The calculated particle sizes of the powders calcined at 320 °C under non-flowing air and at 450 °C under flowing air are 90 and 80 nm.

Table 3
The specific surface areas of the powders calcined at different temperatures under different atmospheres (m^2/g)

	Temperature (°C)								
	220	270	320	350	400	450	500	550	650
Under non-flowing air	2.8	–	8.7	5.9	–	–	–	4.0	–
Under flowing nitrogen	–	–	2.6	3.2	–	–	–	4.4	3.6
Under flowing air	4.6	3.7	3.0	2.8	3.5	9.8	7.6	5.6	2.8

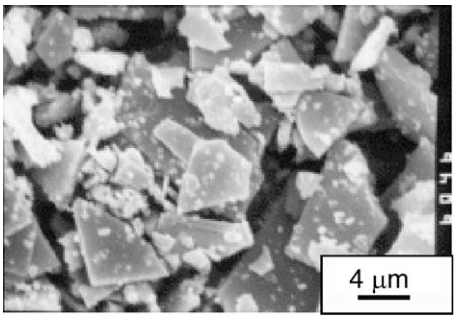

Fig. 7. SEM micrograph of the precursor used in this study.

Fig. 7 shows the SEM micrograph of the precursor. The particle size of the precursor was several microns. Precursor particles are broken into many small particles during decomposition. Fig. 8 shows the SEM micrograph of calcined powder at 320 °C under non-flowing air, from which can been seen that the precursor particle has broken into many smaller particles. The specific surface area decreases due to agglomeration of small particles during calcination of the samples at high temperatures, and the particles still maintained the shape of the precursor, as shown in Fig. 9. The increase in the density from precursor into amorphous or oxide powder results in the internal shrinkage, leads to the formation of pores and cracks. At lower temperatures, the specific surface area of calcined powder increases with increasing temperature due to the formation of pores and cracks. In the temperature range of amorphous powder formation, the specific surface area decreases with increasing temperature due to agglomeration of small particles. At temperatures higher than 300 °C, the transformation of amorphous powder into crystalline powder starts. Hence, the specific surface area increases. The maximum specific surface area was obtained when the calcination was done at 450 °C.

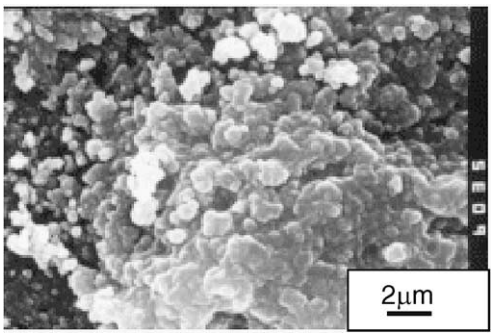

Fig. 8. SEM micrograph of the powder calcined at 320 °C under non-flowing air.

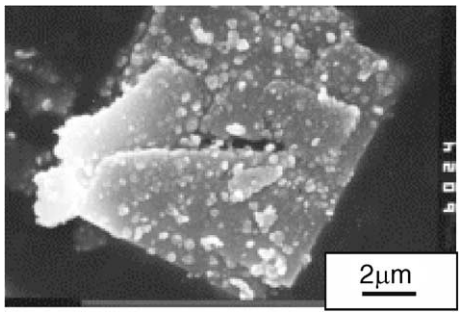

Fig. 9. SEM micrograph of the powder calcined at 550 °C under non-flowing air.

The specific surface area of the powders calcined under flowing gases was similar. However, the specific surface area of the powders calcined under non-flowing gas was different. Crystalline powders were obtained under non-flowing air, while mainly amorphous powders were obtained under flowing air or nitrogen in the same temperature range. Therefore, a maximum of specific surface area was achieved by calcination at 320 °C, where the transformation from amorphous into crystalline takes place.

4. Conclusions

1. The particle size of precursor could be reduced more than 10 times after calcination. Particle sizes of around 80 and 90 nm have been obtained in the powders calcined at 450 °C under flowing air and at 320 °C under non-flowing air, respectively. By calcining the powder from low temperature to high temperature, two transformations occur, i.e. crystalline into amorphous powder and then amorphous into crystalline powder again. The surface area is largest at the temperature of amorphous powder transformation into crystalline powder. To achieve the smallest particle size, the calcination temperatures of 320 and 450 °C are suggested under non-flowing air and flowing air, respectively.
2. The calcination of the powder can be controlled to produce an amorphous powder or crystalline

powder at the same temperature by varying the gas phase composition during the calcination in medium temperature range. The decomposition of the precursor, $(NH_4)_5Co_{2.5}(NH_3)_{2.5}H_2W_{12}O_{42}\cdot 9H_2O$, can be divided into five different steps. The properties of the powder produced are dependent on the composition of the gas phase. In general, the precursor decomposed into oxides (main composition $CoWO_4$ and WO_3) under 520 °C in air with a total weight loss of 10.3%.

3. The precursor calcined in different gas phases showed different decomposition behaviour and consequently gives different products. The decomposition of the precursor at medium and high temperatures varied with the gas phase composition due to the effect of different oxygen content in the gas phase. The higher oxygen content could accelerate the decomposition of the precursor. The decomposition of the precursor finished at the lowest temperatures in flowing air, while the decomposition of the precursor finished at higher temperatures in flowing nitrogen.

Acknowledgements

Authors would like to thank Mr. Sverker Wahlberg, Materials Chemistry Division, Royal Institute of Technology, Stockholm, for his help during this work.

References

[1] W.D. Schubert, E. Lassner, Int. J. Refract. Met. Hard Mater. 10 (1991) 133.
[2] J.W. van Put, T.W. Zegers, H. Liu, Int. J. Refract. Met. Hard Mater. 10 (1991) 123.
[3] A. Lackner, A. Filzeieser, P. Paschen, W. Köck, Int. J. Refract. Met. Hard Mater. 14 (1996) 383.
[4] Z. Zou, C. Qian, E. Wu, Y. Chang, Int. J. Refract. Met. Hard Mater. 1 (1988) 57.
[5] A. Lackner, T. Molinari, P. Paschen, Scand. J. Metall. 25 (1996) 115.
[6] A.K. Basu, F.R. Sale, J. Mater. Sci. 12 (1977) 1115.
[7] W.D. Schubert, E. Lassner, Int. J. Refract. Met. Hard Mater. 10 (1991) 171.
[8] N.E. Fouad, A.K.H. Nohman, M.I. Zaki, Thermochim. Acta 239 (1994) 137.
[9] G.J. French, F.R. Sale, J. Mater. Sci. 16 (1981) 3427.
[10] L. Bartha, A. Kiss, J. Neugebauer, T. Nemeth, High Temp.-High Press. 14 (1982) 1.
[11] E. Lassner, W.D. Schubert, Int. J. Refract. Met. Hard Mater. 13 (1995) 111.
[12] H.J. Scussel, Friction and wear of cemented carbides, in: S.D. Henry (Ed.), ASM Handbook—Friction, Lubrication and Wear Technology, vol. 18, ASM International, USA, 1992, p. 795.
[13] L.E. Mccandlish, B.H. Kear, B.K. Kim, Mater. Sci. Technol. 6 (1990) 953.
[14] Z. Fang, J.W. Eason, Int. J. Refract. Met. Hard Mater. 13 (1995) 297.
[15] B.K. Kim, G.H. Ha, D.W. Lee, J. Mater. Process. Technol. 63 (1997) 317.
[16] Z. Zhang, S. Wahlberg, M. Muhammed, Nanostruct. Mater. 12 (1999) 163.
[17] B.H. Kear, L.E. Mccandlish, Nanostruct. Mater. 3 (1993) 19.
[18] L.E. Mccandlish, B.H. Kear, S.J. Bhatia, US Patent 5 352 269 (1994).
[19] L.E. Mccandlish, B.H. Kear, B.-K. Kim, US Patent 5 651 808 (1997).
[20] I. Keizo, et al., US Patent 3 440 035 (1969).
[21] M. Muhammed, S. Wahlberg, I. Grenthe, US Patent 5 594 929 (1997).
[22] I. Grenthe, M. Muhammed, S. Wahlberg, US Patent 5 632 824 (1997).
[23] Y.T. Zhu, A. Manthiram, Composites B 27B (1996) 407.
[24] Z. Zhang, Y. Zhang, M. Muhammed, Int. J. Refract. Met. Hard Mater. 20 (2002) 227.
[25] N.E. Fouad, A.K.H. Nohman, M.I. Zaki, Thermochim. Acta 343 (2000) 139.
[26] N.E. Fouad, A.K.H. Nohman, M.A. Mohamed, M.I. Zaki, J. Anal. Appl. Pyrol. 56 (1) (2000) 23.
[27] J.W. van Put, T.W. Zegers, H. Liu, Int. J. Refract. Met. Hard Mater. 13 (1995) 61.
[28] E. Lassner, W. Schubert, TUNGSTEN, Properties, Chemistry, Technology of the Element, Alloys, and Chemical Compounds, Kluwer Academic Publishers/Plenum Press, Dordrecht/New York, 1999.
[29] R.C. Weast (Ed.), Handbook of Chemistry and Physics, 60th ed., CRC Press, Boca Raton, 1979–1980, p. B-74.